The Effect of Solute Dissolution Kinetics on Cloud Droplet Formation: Extended Köhler theory

A. Asa-Awuku[1] and A. Nenes[1, 2 *]

[1]School of Chemical and Biomolecular Engineering, Georgia Institute of Technology, Atlanta, GA, 30332

[2]School of Earth and Atmospheric Sciences, Georgia Institute of Technology Atlanta, GA, 30332

[*]Corresponding author

Abstract

This study focuses on the importance of solute dissolution kinetics for cloud droplet formation. To comprehensively account for the kinetics, a numerical model of the process was developed. Simulations of cloud droplet growth were performed for solute diffusivity, droplet growth rates, dry particle and droplet diameters relevant for ambient conditions. Simulations suggest that high ambient supersaturations and low solute diffusivity are major contributors to significant decreases in effective solute surface concentrations during droplet growth. The numerical simulations were incorporated into Köhler theory to assess the impact of dissolution kinetics on the droplet equilibrium vapor pressure. The modified Köhler theory implies that only CCN with slowly dissolving solute could have a "dynamical" equilibrium saturation ratio that is considerably different from that obtained using thermodynamic equilibrium arguments alone.

1 Introduction

Organics constitute a major component of natural and anthropogenic particulate matter (Sloane, 1991; Wolff, 1991; Chow, 1994; Seinfeld and Pandis, 1998), yet much remains to be grasped about their effects on cloud droplet formation. Although not completely understood, carbonaceous aerosol can readily form cloud droplets (Novakov and Penner, 1993) and potentially have a strong effect on cloud formation and the hydrological cycle (Shulman et al., 1996; Facchini et al., 1999; IPCC, 2001; Feingold and Chuang, 2002; Nenes et al., 2002; Lance et al., 2004).

The theory used to describe the formation of cloud droplets from precursor aerosol, or, "cloud condensation nuclei" (CCN), was first developed by Köhler (Köhler, 1936) and has successfully been applied to CCN composed of deliquescent inorganic salt aerosols (e.g., ammonium sulfate and sodium chloride) and low molecular weight organic species that exhibit hygroscopic behavior (e.g., adipic acid and glutaric acid) (Cruz and Pandis, 1997; Raymond and Pandis, 2002). Unfortunately, the theory is less successful in describing the behavior of less hygroscopic compounds (Cruz and Pandis, 1997; Raymond and Pandis, 2002). Analysis of ambient CCN measurements (Chuang P. Y., 2003; VanReken, 2003) can show large deviations (often attributed to the complex interaction of organics with water) between predicted and measured CCN concentration under polluted conditions. Organics, depending on their solubility, can contribute solute (Shulman et al., 1996; Laaksonen et al., 1998). Hydrophobic compounds with multiple functional groups may act as strong surfactants and considerably depress surface tension (Shulman et al., 1996; Facchini et al., 1999; Nenes et al., 2002); compressed surfactant

layers may act as “film-forming compounds”, and may influence droplet growth kinetics enough to affect droplet number and spectral dispersion (Blanchard, 1964; Gill et al., 1983; Feingold and Chuang, 2002; Nenes et al., 2002; Chuang P. Y., 2003). Polymerization reactions, thought to occur in secondary organic aerosol (Limbeck et al., 2003), may also have a considerable impact on their CCN properties (VanReken et al., 2005). All the effects combined give a wide and complex range of effects on CCN and cloud droplet formation (Nenes et al., 2001). A thorough review of organics and their interactions with water vapor can be found in Kanakidou et al., (2005).

A common assumption for partially soluble compounds is that solute instantaneously dissolves and distributes uniformly throughout the drop (Laaksonen et al., 1998; Raymond and Pandis, 2002; Shantz et al., 2003). Compared to electrolytes, the majority of organic compounds are not very soluble in water, do not deliquesce, have a higher molar mass and thus diffuse more slowly in aqueous solutions. The implication for a growing droplet is that mass transfer of the dissolving organics may not be fast enough to assure uniform distribution of solute through the droplet volume; this kinetic limitation may decrease the solute concentration at the droplet surface and increase the droplet equilibrium vapor pressure. If sufficient, the latter may delay or even hinder droplet formation. Thus, assuming instantaneous dissolution and distribution of solute throughout the droplet volume may overestimate the effect of slightly soluble compounds on CCN activation. The kinetic limitation mechanism identified alone is fundamentally different from the growth delay identified by Shantz et al. (2003), which arises from differences in the equilibrium curves between inorganic and organic CCN. It should be noted that even though diffusion of electrolytes may not be important for cloud droplet formation, it

could be important during their deliquescence. Lehtinen et al., (2003) examined this problem experimentally and theoretically; they concluded that the water equilibration timescale for NaCl particles may be large (even hours), depending on their dry size.

This study focuses on exploring the effects of solute dissolution kinetics on cloud droplet formation. A numerical model is developed to simulate the dissolution of solute from a solid core located at the center of the droplet and its diffusion throughout the aqueous phase of the growing drop. Conditions are determined for which a significant decrease in surface solute concentration is expected. The numerical simulations are parameterized and introduced into Köhler theory for a thorough analysis of dissolution kinetics on CCN activity.

2 Dissolution kinetics model

2.1 Equation formulation

The numerical model is based on conservation of mass for the dissolving substance in a spherically symmetric droplet. The solute originates from a spherical solid core located at the center of the droplet; after dissolution, we assume that the solute mass transport occurs (via molecular diffusion) from the core to the droplet surface. Chemical reactions could also take place that would further delay dissolution, but considering such effects is compound-specific and beyond the scope of this study. Convective transport within the droplet phase is neglected, because *i*) the solution is assumed to be dilute, and, *ii*) the low terminal velocity for droplets smaller than 20 μm in diameter (i.e., most CCN during their activation phase) yields negligible shear forces on their surface (Seinfeld and Pandis, 1998). Assuming that the solid core is composed of a slightly soluble substance *A*, the

dissolution and transport of solute from the core into the droplet aqueous phase can be described by,

$$\frac{\partial C_A(t,r)}{\partial t} = D_{Aw}\left[\frac{1}{r^2}\frac{\partial}{\partial r}\left(r^2\,\frac{\partial C_A(t,r)}{\partial r}\right)\right] \tag{1}$$

where $C_A(t,r)$ denotes the concentration of A at time t and distance r from the core droplet center, and D_{Aw} is the diffusivity of A in water. D_{Aw} depends on temperature and solute molecular size, but typically ranges between 10^{-9} and 10^{-10} m^2s^{-1} (Table 1).

The concentration of A throughout the droplet volume is initially equal to its solubility in water, C^{eq},

$$C_A(0,r) = C^{eq} \tag{2}$$

In terms of spatial boundary conditions, we assume that the solution is saturated with A at the core-solution interface, located at $r = R_c$.

$$C_A(t>0, R_c) = C^{eq} \tag{3}$$

If the core is small enough, C^{eq} could increase because of the Kelvin effect; this solubility enhancement is important when the core is small and the interfacial energy between the core and water (contact angle) is large (i.e., the compound is hydrophobic). Given that many of the slightly soluble compounds are hydrophilic with an almost zero contact angle, the interfacial energy is close to zero, so the solubility enhancement is important only at extremely small core sizes, where most of the core is dissolved. We therefore neglect curvature effects on Equation 3.

The boundary condition at the droplet surface is somewhat more complex, as solute diffusion and water condensation affect the surface concentration of A. The $C_A(t,R_p)$

tendency at the droplet surface can be rewritten in terms of the rate of change of freshly condensed water volume, $\frac{dV}{dt}$ and the molar flux $\frac{dn_A}{dt}$ of A into V,

$$\frac{dC_A(t,R_p)}{dt} = \frac{d}{dt}\left[\frac{n_A}{V}\right] = \frac{-n_A}{V^2}\left(\frac{dV}{dt}\right) + \frac{1}{V}\left(\frac{dn_A}{dt}\right) = \frac{-C_A(t,R_p)}{V}\left(\frac{dV}{dt}\right) + \frac{1}{V}\left(\frac{dn_A}{dt}\right) \quad (4)$$

The freshly condensed water (hereon referred to as the "surface layer") is assumed to occupy a layer of infinitesimal thickness, *dr*, adjacent to the droplet surface. $\frac{dV}{dt}$ is equal to the rate of change of droplet volume and can be expressed in terms of the droplet diameter, D_p, as

$$\frac{dV}{dt} = \frac{\pi {D_p}^2}{2} \cdot \frac{dD_p}{dt} \quad (5)$$

$\frac{dn_A}{dt}$ is equal to the flux of solute from the bulk of the droplet,

$$\frac{dn_A}{dt} = -D_{Aw}\frac{\partial C_A(t,R_p - dr)}{\partial r} 4\pi (R_p - dr)^2 \approx -D_{Aw}\frac{\partial C_A(t,R_p)}{\partial r}\pi {D_p}^2 \quad (6)$$

In equation (6), we assumed that the surface layer has negligible thickness compared to the droplet radius, so that $R_p - dr \approx R_p$. Introducing Equations (5) and (6) into (4) yields,

$$\frac{\partial C_A(t,R_p)}{\partial t} = \frac{-3}{D_p}\left[C_A(t,R_p)\frac{dD_p}{dt} + 4D_{Aw}\frac{\partial C_A(t,R_p)}{\partial D_p}\right] \quad (7)$$

Equation (7) expresses the rate of change of C_A at the growing droplet surface and is an exact boundary condition for equation (1). $\frac{dD_p}{dt}$ can be written in terms of the ambient conditions (Seinfeld and Pandis, 1998) as,

$$\frac{dD_p}{dt} = \frac{1}{D_p}\frac{(S - S_{eq})}{G} \tag{8}$$

where $S = \frac{p^w}{p^o(T)}$ is the ambient saturation ratio, p^w is the water vapor partial pressure, $p°(T)$ is the water saturation vapor pressure at the ambient temperature T and S_{eq} is the equilibrium saturation ratio of the growing droplet. G is a kinetic growth parameter defined as $\frac{\rho_w RT}{4p°(T)D'_v M_w} + \frac{\Delta H_v \rho_w}{4k_a' T}\left(\frac{\Delta H_v M_w}{TR} - 1\right)$ where M_w and ρ_w are the molecular weight and density of water, respectively, R is the universal gas constant, ΔH_v is the latent heat of vaporization for liquid water, k_a' is the thermal conductivity of air, and D_v' is mass transfer coefficient of water vapor from the gas to the droplet. If $S_{eq} \approx 1$ (this assumption will be relaxed in section 3.2) and if we neglect the size-dependence of G, Equation (8) is inversely proportional to D_p and simplifies to:

$$\frac{dD_p}{dt} \approx \frac{1}{G}\frac{S-1}{D_p} = \frac{1}{G}\frac{s}{D_p} \tag{9}$$

where $s = S - 1$ is the ambient water vapor supersaturation. Substitution of Equation (9) into Equation (7) gives,

$$\frac{\partial C_A(t,R_p)}{\partial t} = \frac{-3}{D_p}\left[\frac{1}{G}\frac{sC_A(t,R_p)}{D_p} + 4D_{Aw}\frac{\partial C_A(t,R_p)}{\partial D_p}\right] \tag{10}$$

Equation (10) is the droplet surface boundary condition used to integrate Equation (1).

2.2 Integration procedure

Equation (1) with the initial and boundary conditions expressed by Equations (2), (3) and (10), is numerically integrated using finite differences. The solution procedure entails applying the initial condition (Equation 2) to all grid points, and then integrating the equations over time using central-differencing in the spatial direction and backward differencing in time. The boundary condition at $r = R_c$ (Equation 3) is directly applied, while the boundary condition at $r = R_p$ (Equation 10) is applied after approximating the derivatives with finite differences:

$$C_A(t+\Delta t, R_p) = C_A(t, R_p) - \frac{3\Delta t}{D_p}\left[\frac{1}{G}\frac{sC_A(t,R_p)}{D_p} + 4D_{Aw}\frac{C_A(t,R_p) - C_A(t,R_p-\Delta r)}{\Delta r}\right] \quad (11)$$

where the "new" time is "t+Δt", the "old" time is "t", and Δt, Δr are the time step and grid spacing, respectively. 5×10^4 grid points between $r = R_c$ and $r = R_p$ are used; the equations are integrated over time until steady-state is achieved.

2.3 Simulations considered

Examination of Equation (1) and its boundary conditions (Equations 2, 3 and 10) suggests that four parameters influence the extent of surface solute concentration depression from dissolution kinetics: D_{Aw}, s, D_p and the core diameter, D_c. We explore the dependence of C_A to these parameters by performing a series of sensitivity simulations. To avoid any effects from transients and initial conditions, we focus on the steady-state profiles of $C_A(t,r)$; thus, to facilitate the numerical integration, we keep R_c and R_p constant during the integration.

Overall, a total of 500 simulations were completed. D_{Aw} was varied between 1×10^{-10} to 1×10^{-9} m s^{-2}, which encompasses the diversity of water-soluble organic compounds found in ambient aerosol (Table 1). Ambient supersaturations were chosen to represent globally important cloud types; we consider radiative fog (s = 0.01%), stratiform (s = 0.25%), cumuliform (s = 0.5%) and convective clouds (s = 1%) (Pruppacher and Klett, 1997; Seinfeld and Pandis, 1998; Nenes et al., 2001). Five different droplet diameters were considered (0.1, 0.5, 1.0, 5.0 and 10 μm) to represent the transition from deliquesced aerosol to activated cloud droplets (Seinfeld and Pandis, 1998). The slightly soluble core size was also varied, expressed as a fraction of the wet diameter (0.5%, 1%, 5%, 10% and 20% of D_p).

2.4 Simulation results

Figure 1 illustrates the characteristics of all numerical simulations. Initially, C_A is uniform throughout the droplet volume, being equal to C^{eq}. As water begins to condense, C_A decreases at the surface layer, progressively diluting much of the droplet volume. This can be seen in Figure 2, which presents transient radial profiles of C_A. Simulations are shown for D_p = 1μm, D_c = 0.01μm, $D_{Aw} = 1\times10^{-10}$ m^2 s^{-1}, and s = 1%. The simulations indicate that throughout most of the simulation, C_A drops steeply with distance from the core until a characteristic distance, R_s (Figure 1), after which the gradient of C_A becomes effectively zero (at steady state). Figure 2 suggests that R_s may not significantly change location, and that the steady-state solution can be achieved in a fraction of a second, i.e. within the timescale of cloud droplet activation. It is therefore sufficient to focus on the steady-state concentration profile, with an emphasis on the steady-state $C_A(t, R_p)$, hereon

referred to as C^*, because it determines the droplet equilibrium vapor pressure. Therefore, it is important to explore the dependence of C^* on all four parameters varied in Table 1.

Figure 3 presents steady-state radial profiles of C^*/C^{eq} for D_{Aw} ranging between 1×10^{-9} and 1×10^{-10} m^2 s^{-1}. Simulations are shown for D_p = 1μm, D_c = 0.01μm and s = 1%. As expected, the most pronounced decrease in C^* occurs for the lowest molecular diffusivity (~10^{-10} m^2 s^{-1}), i.e., when diffusion is the slowest. The simulations suggest that the concentration depression is minor (~ 5%) for high diffusivity (D_{Aw} = 10^{-9} m^2 s^{-1}) but becomes significant (>10%) for $D_{Aw} < 5\times10^{-10}$ m^2 s^{-1}. The depression in C^* seems to be inversely proportional to D_{Aw}.

In addition to D_{Aw}, C^* depends on the droplet growth rate (i.e., the ambient supersaturation). This is depicted in Figure 4, which presents steady-state radial profiles of C^*/C^{eq} for s ranging between 0.1% and 1%. Simulations are shown for D_p = 1μm, D_c = 0.01μm, $D_{Aw} = 1\times10^{-9}$ m^2 s^{-1}. The largest drop in C^* is seen for high s, as this is the condition for which dilution of A from water condensation at the surface layer is strongest. Compared to D_{Aw} (Figure 3), an order of magnitude change in s leads to a smaller (but still significant) decrease in C^*.

Finally, C^* depends on the droplet and core diameters. This is depicted in Figure 5, which shows C^*/C^{eq} as a function of core diameter and ambient supersatuation. Simulations are shown for (a) D_p = 1μm, $D_{Aw} = 1\times10^{-10}$ m^2 s^{-1}, and, (b) D_p = 5μm, $D_{Aw} = 1\times10^{-9}$ m^2 s^{-1}. It is clear that decreasing the core size and increasing the droplet size depress C^*,

because mass transport becomes less efficient in supplying solute at the droplet surface. Simulations suggest that $C*$ can be as much as fifty percent lower than C^{eq}.

The trends seen for C^* in the simulations can be rationalized through the following analysis. Applying the steady state requirement on the droplet surface boundary condition (Equation 10),

$$0 = -\frac{3}{D_p}\left[C_A(t,R_p)\left(\frac{dD_p}{dt}\right) + 4D_{Aw}\left(\frac{dC_A(t,R_p)}{dD_p}\right)\right] \tag{12}$$

$\left(\frac{dC_A(t,R_p)}{dD_p}\right)$ refers to the gradient of C_A at the droplet surface, and can be expressed as $\left(\frac{dC_A(t,R_p)}{dD_p}\right) \approx \frac{C^* - C^{eq}}{\Delta D_p}$, where ΔD_p is an appropriate spatial scale (more on ΔD_p will be discussed in section 3.1). Substitution of the above into Equation (8) and solving for C^* yields,

$$C^* = \frac{C^{eq}}{\frac{\Delta D_p}{4 \cdot D_{Aw}}\left(\frac{dD_p}{dt}\right)+1} \tag{13}$$

Substituting Equation (9) into (13) gives,

$$C^* = \frac{C^{eq}}{\frac{s}{4 \cdot D_{Aw} G}\left(\frac{\Delta D_p}{D_p}\right)+1} \tag{14}$$

Equation 14 confirms the numerical simulation trends; when D_{Aw} is large, $C^* \approx C^{eq}$ and when it decreases, $C^* < C^{eq}$. Similarly, smaller droplet sizes or large ambient supersaturations yield large growth rates, and will decrease C^* because of excessive dilution of the surface layer. However for low ambient supersaturations or large droplet

diameter, $\frac{dD_p}{dt}$ is negligible and $C^* \approx C^{eq}$. D_c also affects C^*; smaller sizes imply that the solute needs to diffuse over a larger distance, hence ΔD_p increases and C^* decreases.

3. Introducing Dissolution Kinetics into Köhler Theory

3.1 Parameterization of the numerical simulations

It is desirable to introduce appropriate modifications to Köhler theory when assessing the effects of solute mass transfer kinetics on cloud droplet formation. This could be accomplished by establishing a relationship between C^* and the dissolution kinetics parameters D_{Aw}, s, D_p and D_c. The steady-state droplet boundary condition (Equation 14) is ideally suited for this purpose; the parameter ΔD_p however must first be defined. In deriving Equation (14), we assumed that $\left(\frac{dC_A(t,R_p)}{dD_p}\right) \approx \frac{C^* - C^{eq}}{\Delta D_p}$. Based on Figure 1, most of the variation of C_A takes place in a region close to the core; therefore the flux of A at the surface of the droplet can, at steady state, can be expressed as,

$$\left.\frac{dC_A(t,R_p)}{dD_p}\right|_{R_p} = \left.\frac{dC_A(t,R_p)}{dD_p}\right|_{Rs} \left(\frac{R_s^2}{R_p^2}\right) \approx \frac{C^* - C^{eq}}{R_s - R_c}\left(\frac{R_s^2}{R_p^2}\right) \qquad (15)$$

where R_s is the distance where the concentration gradient becomes effectively zero (Figure 1). Defining $\omega = \frac{D_p}{D_c}$ and $\delta = 1 - \frac{D_c}{D_s}$ (where D_s and D_p are diameters corresponding to R_s and R_p , respectively), Equation (15) becomes,

$$C^* = \frac{C^{eq}}{1 + \delta(1-\delta)\dfrac{\omega s}{4GD_{Aw}}} \tag{16}$$

Equation (16) describes the solute surface concentration at the droplet surface in terms of solubility, ambient supersaturation, solute diffusivity, droplet and core size, and the non-dimensional coefficient δ which is related to the mass transfer kinetics. In agreement with the numerical simulations, Equation (16) indicates that a decrease in solute diffusivity and an increase ambient supersaturation both yield a decrease in the solute surface concentration. A small core size (i.e., increasing ω) implies that the solute has to diffuse over a large distance; C^* will decrease because water vapor condensation is more efficient in diluting the droplet surface layer. We use the numerical simulations to constrain δ so that Equation (16) reproduces the steady-state C^* derived from the simulations. Least squares minimization yields $\delta(1-\delta)$=0.8 with which the numerical simulations are reproduced to within 10% (Figure 6).

An issue arises for small core diameters; as the core dissolves and approaches zero, $\omega \to \infty$; under such conditions, Equation (16) predicts that $C^* \to 0$. This is of course does not happen in reality but arises because Equation (16) was derived assuming steady-state for $C_A(t,r)$. When $D_c \to 0$, the steady-state timescale becomes exceedingly long, and Equation (16) is not applicable. This limitation is easily overcome by considering the droplet growth dynamics: Initially, droplet growth is at a rate that steady state assumptions can be made; the core begins to dissolve, shrink and eventually reaches a size in where Equation (16) is not applicable. At this instance, we will assume that C^* does not change anymore; thus a lower-limit constraint is applied on C^*. We consider a timescale relevant for cloud droplet formation is ~ 1 sec; under this constraint, numerical

simulations suggest that $C^* \geq 0.5C^{eq}$. Therefore, the surface concentration of solute when mass transfer kinetics are considered is parameterized as,

$$C^* = \max\left\{0.5C^{eq},\ \frac{C^{eq}}{1+0.8\frac{\omega s}{4GD_{AB}}}\right\} \tag{17}$$

Although including a lower limit for C^* is introduced to avoid a singular solution, it will be shown (Section 3.4) that neglecting it may not impact calculation of Köhler curves.

3.2 Introduction to Köhler theory

Solute mass transfer kinetics can be included in Köhler theory by appropriate modifications to existing theory. Assuming instantaneous dissolution for slightly soluble compounds, the equilibrium supersaturation, s_{eq}, of a CCN composed of a completely soluble, s, and a slightly soluble fraction, ss, can be expressed as (Shulman et al., 1996),

$$s_{eq} = \frac{4M_w\sigma_w}{RT\rho_w D_p} - \frac{6n_s M_w \upsilon_s}{\pi\rho_w {D_p}^3} - \frac{6n_{ss} M_w \upsilon_{ss}}{\pi\rho_w {D_p}^3} \tag{18}$$

where n_s, n_{ss} represents the moles of solute dissolved in the droplet from the soluble and slightly soluble species, respectively; $\upsilon_s, \upsilon_{ss}$ are the corresponding "effective" van't Hoff factors.

If the solubility of ss, C^{eq}, is expressed in moles m^{-3}, then in the presence of a soluble core (i.e., when there is not enough water in the CCN to completely dissolve the core) Equation (18) becomes,

$$s_{eq} = \frac{4M_w\sigma_w}{RT\rho_w D_p} - \frac{6n_s M_w \upsilon_s}{\pi\rho_w {D_p}^3} - \frac{M_w}{\rho_w} C^{eq} \upsilon_{ss} \tag{19}$$

If the core is completely dissolved, Equation (18) is used with n_{ss} equal to n_{ss}^{tot}, the total moles of slightly soluble species available in the CCN. Solute transport kinetics is introduced in Equation (19) by replacing C^{eq} with C^{*} (Equation 17), modified slightly to relax the assumption that $S_{eq} \cong 1$,

$$s_{eq} = \frac{4M_w\sigma_w}{RT\rho_w D_p} - \frac{6n_s M_w \upsilon_s}{\pi\rho_w D_p^{\,3}} - \frac{M_w}{\rho_w}\upsilon_{ss} \max\left\{0.5C^{eq},\ \frac{C^{eq}}{1+0.8\dfrac{\omega(s-s_{eq})}{4GD_{AB}}}\right\} \qquad (20)$$

The term (s-s_{eq}) is termed "oversaturation" and expresses the driving force for growth in Equation (9) when the CCN is smaller than its critical diameter; the implication is that the Kölher curve becomes implicit (a second order polynomial) with respect to s_{eq}. We assume that if the core has completely dissolved, Equation (18) is used with n_{ss}=n_{ss}^{tot}. This implies that mass transfer kinetics are not considered after the core has completely dissolved; in reality there is a relaxation time associated with solute transport from the bulk of the droplet to the surface layer, which for simplicity we have neglected.

Equation (20) contains kinetic information; nevertheless, it expresses the equilibrium vapor pressure of the growing droplet, hence is still a "Köhler curve". Equation (20) would not be applicable if the assumption of chemical equilibrium between the droplet surface layer and the adjacent vapor (which is almost instantaneous) were not satisfied. This is not the case, as surface concentration changes are driven by the droplet growth kinetics, hence are driven by its timescale, which is much longer than required for surface equilibration. The difference between Equation (20) and more "traditional" Köhler theory is that the chemical potential of water in the bulk of the droplet is different from that at the surface (and drives the mass transfer of solute throughout the droplet).

When applying Equation (20), the undissolved core diameter (or radius) needs to be computed. This can be done from the solute mass balance, provided that n_{ss}^{tot} is known. Assuming that the core is composed exclusively of slightly soluble material, R_c is calculated from

$$R_c = \left\{ \frac{3}{4\pi} \frac{M_{ss}}{\rho_{ss}} \left(n_{ss}^{tot} - n_{ss} \right) \right\}^{1/3} = \left\{ \frac{3}{4\pi} \frac{M_{ss}}{\rho_{ss}} \left(n_{ss}^{tot} - 4\pi \int_{R_c}^{R_p} r^2 C_{ss}(t,r) dr \right) \right\}^{1/3} \tag{21}$$

where M_{ss}, ρ_{ss} are the slightly soluble molar mass and density, respectively. In calculating $n_{s,s}$ the steady-state concentration profile $C_{ss}(t,r)$ is given by,

$$C_{ss}(t,r) = \frac{\left(C^* - C^{eq} \right) R_p}{\left(R_c - R_p \right)} \left[\frac{R_c}{r} + 1 \right] + C^{eq} \tag{22}$$

Substitution of Equation (22) into (21) and integration yields an algebraic equation that is numerically solved for R_c.

3.3. Effect of dissolution kinetics on equilibrium supersaturation

Figure 7 displays Köhler curves with and without the effect of solute dissolution kinetics. In these calculations, the dry CCN is 100 nm in diameter and composed of a partially soluble substance with 1750 kg m^{-3} density, 0.132 kg mol^{-1} molar mass (similar to that of glutaric acid), van't Hoff factor of 2 and a solubility of 10^{-2} kg kg^{-1}. Ambient supersaturation is assumed to be 1.0%. Assuming that dissolution and mass transfer of the solute is instantaneous (blue curves) yields a "typical" Köhler curve (Figure 7a). At small wet diameters, the amount of liquid water is insufficient to completely dissolve the core, hence the concentration of solute is constant throughout the droplet volume until complete dissolution (here at ~0.56 μm). For larger wet diameters, the droplet dilutes as it

grows and develops the characteristic "Köhler" maximum in s_{eq}. When dissolution kinetics are considered, the decrease in C^* (Equation 17) "shifts" s_{eq} to higher levels at small wet diameters; this effect is negligible for large solute diffusivity (> 5×10^{-10} m^2 s^{-1}) but becomes modest for low diffusivity (< 2.5×10^{-10} m^2 s^{-1}). Here, the effect on s_{eq} can be ~10% for D_A= 5×10^{-10} m^2 s^{-1}, but as large as 70% for smaller values of the coefficient. The effect of dissolution kinetics is also clearly seen on the core diameter and amount of dissolved solute (Figure 7b); as dissolution kinetics require a finite time to redistribute soluble material throughout the droplet volume, core is present for a wider range of wet diameters and thus can even influence the region beyond the "traditional" critical diameter. For example, at 0.56 μm wet diameter the core is practically dissolved for instantaneous to large solute diffusivity (>5×10^{-10} m^2 s^{-1}), while only 70% (i.e., a core more than half its dry size) is dissolved at lower diffusivity. Thus, appreciable amounts of core can be present at droplet sizes between 0.5 and 1 micron; conditions can be found for which core is seen at even larger sizes (not shown).

In addition to the shape of the Köhler curve, dissolution kinetics may also impact the critical supersaturation (i.e., its global maximum), especially when the CCN contains small amounts of soluble salts. This is shown in Figure 8, which displays Köhler curves with (solid lines) and without (shaded lines) the effect of solute dissolution kinetics; the CCN considered have a dry diameter of 100 nm and are composed of a mixture of NH_4HSO_4 and a partially soluble substance with the properties of Figure 7. Ambient supersaturation, s, is assumed to be 1.0%, and D_{Aw} = 7.5×10^{-11} m^2 s^{-1}. When the sulfate mass fraction ranges between 0.05 and 0.1, the critical supersaturation, s_c, of the CCN increases substantially, between 2 and 5%. For higher sulfate mass fractions, s_c increases

are negligible. This behavior can be explained by comparing the concentration of salt and slightly soluble substance around the critical diameter, D_{crit}. If there is very little sulfate present, then D_{crit} is close to the particle dry diameter, so dissolution kinetics have a minor effect on s_c; when there is significant amounts of sulfate, the slightly soluble compound (and its concentration variations thereof from dissolution kinetics) does not significantly impact the Raoult term of the Köhler curve. Only when both components yield comparable concentrations about the D_{crit}, can concentration variations from dissolution kinetics have an appreciable impact on the equilibrium vapor pressure. It should be noted that even when s_c is not affected, the shape of the Köhler curve (hence the droplet growth kinetics) may substantially change if dissolution kinetics are slow enough (Figure 8).

3.4. Is a minimum C^* required for Köhler curve calculation?

When developing Equation (20), a minimum limit for C^* was considered to avoid a singular solution. However, *i*) C^* in Equation (16) scales with R_p^{-1}, while dilution from condensation scales with R_p^{-3}, *ii*) enhancement of C^{eq} from curvature effects (section 2.1) may limit C* from approaching zero, and, *iii*) core dissolution occurs when droplet diameter increases; this decreases the growth rate and increases C^* (Equation 14). All suggest that incorporating dissolution kinetics into Köhler theory may not be sensitive to the minimum value of C^*; a lower limit for C^* may not even be required. This is explored below.

Figure 9 displays C^* as a function of wet diameter and minimum C^*. The CCN composition and size is similar to Figure 7, while $D_{Aw} = 7.5\times10^{-11}$ m^2 s^{-1}, and ambient supersaturation is set to 1%. The inset graph presents the corresponding Köhler curves.

Minimum C^* values considered are $1.0C^{eq}$ (i.e., instantaneous dissolution), 0.95 C^{eq}, $0.5C^{eq}$, $0.25C^{eq}$, and 0.0 C^{eq} (i.e., no lower limit is posed). As expected, instantaneous dissolution (dark blue curve) yields the C^* profile expected from "traditional" Köhler theory: while a core exists (i.e., $D_p < 0.56$ μm), C^* is constant and equal to C^{eq}. After dissolution, C^* scales with D_p^{-3} because of droplet dilution. For $C^* \geq 0.95C^{eq}$ (light blue curve), C^* originally decreases as water condenses on the droplet, but very soon approaches the limit; C^* subsequently remains constant until the core completely dissolves, beyond which C^* scales with D_p^{-3}. The corresponding Köhler curve is essentially identical to the "traditional" calculation. For all of the other lower limits examined, a common behavior is seen: C^* drops in accordance with Equation (16) and smoothly transitions (when about 70% of the core mass is dissolved) to a D_p^{-3} dependence. C^* collapses to a common curve for all of the lower limits examined; this confirms that the singularity associated with Equation (16) does not affect the calculation of Köhler curves. Although conditions may be found where a minimum C^* may be required, it is likely that for most conditions relevant for atmospheric CCN, a lower limit for C^* may not be necessary.

4 Summary and implications for cloud droplet formation

Partially soluble substances, although able to affect CCN activity, need a finite time to dissolve and redistribute throughout the droplet volume. The importance of dissolution kinetics is the focus of this study. To comprehensively account for the kinetics, a numerical model of the process was developed assuming that diffusion is the primary mechanism of solute transport. Simulations of cloud droplet growth were performed for

ambient ranges of solute diffusivity, droplet growth rates, dry particle and droplet diameters. Simulations suggest that high ambient supersaturations and low solute diffusivity (typical of large organic molecules) can decrease the effective solute surface concentrations by as much as 50%. The steady-state numerical simulations were then parameterized and incorporated into Köhler theory to assess the impact of dissolution kinetics on the droplet equilibrium vapor pressure. Assuming diffusional dissolution and steady-state conditions provides a most conservative assessment of dissolution kinetics; our approach allows for its efficient parameterization and incorporation into Köhler theory.

The modified Köhler theory indicates that if solute dissolution is slow enough, CCN could have a "dynamical" equilibrium saturation ratio that is appreciably higher from that obtained using purely thermodynamic equilibrium arguments. Based on our analysis, compounds with $D_{Aw} > 5\times10^{-10}$ m^2 s^{-1} will not experience significant changes in the Köhler curve from mass transfer kinetics. This is consistent with the finding that CCN composed of soluble electrolytes and low molecular weight organics tend to follow Köhler theory (e.g., Raymond and Pandis, 2002; Cruz and Pandis, 1997); although deliquesced aerosol do not have a solute "core" during droplet activation, our analysis still applies, since the region about the center of the droplet can be much more concentrated with solute and virtually as a "core". However, for higher molecular weight compounds (e.g., HULIS) and low temperatures, where diffusivity is low (i.e., $D_{Aw} \leq 2.5\times10^{-10}$ m^2 s^{-1} and below), mass transfer kinetics may impact equilibrium vapor pressure; this can contribute to the discrepancy often reported between theoretical predictions (i.e., underestimation of s_c) and observations of CCN activity and growth

kinetics. In terms of laboratory experiments, dissolution & mass transfer kinetics may also in part explain why activation curves for organic CCN (i.e., measurements of the ratio between activated CCN and total condensation nuclei as a function of particle size) tend to be broader than for inorganic and low molecular weight CCN.

In terms of ambient CCN, solute dissolution kinetics may not affect s_c if the CCN contains substantial amounts of inorganic electrolytes and low molecular weight organic acids. Conversely, solute dissolution kinetics may influence droplet formation when (a) a partially soluble core is present during the CCN activation, and, (b) the partially soluble solute constitutes a significant fraction of the total solute. In the atmosphere, such particles could correspond to biogenic and secondary organic aerosol (VanReken et al., 2005). If slow enough, dissolution kinetics may also help explain why CCN and cloud droplet number closure studies for ambient aerosol (e.g., Medina et al., 2007; Fountoukis et al., 2007; Ervens et al., 2007) suggest that organics behave as "insoluble"; even if soluble, dissolved organics may diffuse too slowly to fully affect the CCN vapor pressure, hence appearing less "soluble" than they really are. Dissolution kinetics become more important with increasing supersaturation and low temperatures, hence their effects are expected to be most prominent for supercooled droplets, pristine stratocumulus and convective clouds.

Although the effect of dissolution kinetics is not sufficient to inhibit CCN activation, affected droplets under certain conditions may experience slower growth and require a higher level of supersaturation to activate. Both effects can influence the water vapor availability during cloud droplet nucleation and feedback into cloud droplet number and spectral width. To assess the importance of such feedbacks, our newly developed theory

needs to be incorporated into a numerical cloud parcel model (e.g., Nenes *et al.*, 2001); this will be the subject of a future study.

Even though the impacts of dissolution kinetics on droplet formation seems to be modest, our analysis presents a conservative estimate of its impacts (given that we assume steady-state diffusion and that only aqueous-phase diffusion limit transfer from the solid to the droplet interface). The additional effects of transients and slower dissolution kinetics at the core interface may lead to an appreciable impact on droplet formation; the framework presented in this study can be expanded to incorporate and explore such effects.

Acknowledgements

This research was supported by a National Science Foundation CAREER Award, a NASA Earth System Science Graduate Student Fellowship and by Georgia Institute of Technology startup funds. We also thank Purvi Patel for her help with simulations and an anonymous reviewer for constructive comments that helped improve the paper.

References

Blanchard, D. C. (1964). Sea-To-Air Transport Of Surface Active Material. Science 146(364): 396-&.

Chow, J. C., Watson, J. G., Fujita, E. M., Lu, Z. Q., Lawson, D. R. and Ashbaugh, L. L. (1994). Temporal and spatial variations of PM 2.5 and PM 10 aerosol in Southern California Air Quality. Atmospheric Environment 28: 2061-2080.

Chuang P. Y. (2003). Measurement of the timescale of hygroscopic growth for atmospheric aerosols. Journal of Geophysical Research 108 (D9): 4282.

Cruz, C. N. and S. N. Pandis (1997). A study of the ability of pure secondary organic aerosol to act as cloud condensation nuclei. Atmospheric Environment 31(15): 2205-2214.

Facchini, M. C., S. Fuzzi, S. Zappoli, A. Andracchio, A. Gelencser, G. Kiss, Z. Krivacsy, E. Meszaros, H. C. Hansson, T. Alsberg and Y. Zebuhr (1999). Partitioning of the organic aerosol component between fog droplets and interstitial air. Journal Of Geophysical Research-Atmospheres 104(D21): 26821-26832.

Facchini, M. C., M. Mircea, S. Fuzzi and R. J. Charlson (1999). Cloud albedo enhancement by surface-active organic solutes in growing droplets. Nature 401(6750): 257-259.

Feingold, G. and P. Y. Chuang (2002). Analysis of the Influence of Film-Forming Compounds on droplet Growth: Implications for Cloud Microphysical Processes and Climate. Journal of Atmospheric Science, 59.

Fountoukis, C., Nenes, A., Meskhidze, N., Bahreini, R., Brechtel, F., Conant, W. C., Jonsson, H., Murphy, S., Sorooshian, A., Varutbangkul, V., R. C. Flagan, and J. H. Seinfeld (2007) Aerosol–cloud drop concentration closure for clouds sampled during ICARTT, Journal Of Geophysical Research-Atmospheres, 112 (D10S30) doi:10.1029/2006JD007272.

Ervens, B., Cubison, M., Andrews, B., Feingold, G., Ogren, J.A., Jimenez, J.L., and Nenes, A. (2007) Prediction of CCN number concentration using Measurements of Aerosol Size Distributions and Composition and Light Scattering Enhancement

due to Humidity, Journal Of Geophysical Research-Atmospheres 112(D10S32), doi:10.1029/2006JD007426

Gill, P. S., T. E. Graedel and C. J. Weschler (1983). Organic Films On Atmospheric Aerosol-Particles, Fog Droplets, Cloud Droplets, Raindrops, And Snowflakes. Reviews Of Geophysics 21(4): 903-920.

IPCC (2001). Climate change: contribution of working group I to the third assessment report of the intergovernmental panel on climate change, Cambridge University Press.

Köhler, H. (1936). The nucleus in and the growth of hygroscopic droplets. Transactions of the Faraday Society 43: 1152.

Laaksonen, A., P. Korhonen, M. Kulmala and R. J. Charlson (1998). Modification of the Kuhler equation to include soluble trace gases and slightly soluble substances. Journal Of The Atmospheric Sciences 55(5): 853-862.

Lance, S., A. Nenes and T. A. Rissman (2004). Chemical and dynamical effects on cloud droplet number: Implications for estimates of the aerosol indirect effect. Journal of Geophysical Research-Atmospheres 109(D22).

Lehtinen, K.E.J., M. Kulmala, P. Ctyroky, T. Futschek, and R. Hitzenberger (2003). Effect of Electrolyte Diffusion on the Growth of NaCl Particles by Water Vapour Condensation, J. Phys. Chem A, 107, 346-350

Limbeck, A., M. Kulmala and H. Puxbaum (2003). Secondary organic aerosol formation in the atmosphere via heterogeneous reaction of gaseous isoprene on acidic particles. Geophysical Research Letters 30(19).

Medina, J., Nenes, A., Sotiropoulou, R.E., Cottrell, L.D., Ziemba, L.D., Beckman, P.J., Griffin, R.J. (2007) Cloud Condensation Nuclei (CCN) closure during the ICARTT 2004 campaign: a) effects of size-resolved composition, Journal Of Geophysical Research-Atmospheres, 112(D10S31) doi:10.1029/2006JD007588

Nenes, A., R. J. Charlson, M. C. Facchini, M. Kulmala, A. Laaksonen and J. H. Seinfeld (2002). Can chemical effects on cloud droplet number rival the first indirect effect? Geophysical Research Letters 29(17).

Nenes, A., S. Ghan, H. Abdul-Razzak, P. Y. Chuang and J. H. Seinfeld (2001). Kinetic limitations on cloud droplet formation and impact on cloud albedo. Tellus Series B-Chemical And Physical Meteorology 53(2): 133-149.

Novakov, T. and J. E. Penner (1993). Large Contribution Of Organic Aerosols To Cloud-Condensation-Nuclei Concentrations. Nature 365(6449): 823-826.

Pruppacher, H. and J. Klett (1997). *Microphysics of Clouds and Precipitation*. Norwell, Massachusetts, Kluwer Academy.

Raymond, T. R. and S. N. Pandis (2002). Cloud activation of single-component organic aerosol particles. Journal of Geophysical Research.

Seinfeld, J. H. and S. N. Pandis (1998). *Atmospheric Chemistry & Physics: From Air Pollution to Climate Change*, John Wiley & Sons.

Shantz, N. C., W. R. Leaitch and P. F. Caffrey (2003). Effect of organics of low solubility on the growth rate of cloud droplets. Journal Of Geophysical Research-Atmospheres 108(D5).

Shulman, M. L., M. C. Jacobson, R. J. Carlson, R. E. Synovec and T. E. Young (1996). Dissolution behavior and surface tension effects of organic compounds in nucleating cloud droplets. Geophysical Research Letters 23(3): 277-280.

Sloane, C. S., Watson, J., Chow, J., Pritchett, L. and Richards, L.W. (1991). Size-segregated fine particle measurements by chemical species and their impact on visibility impairment in Denver. Atmospheric Environment 25A: 1013-1024.

VanReken, T., Rissman, TA, Roberts, GC, et al. (2003). Toward aerosol/cloud condensation nuclei (CCN) closure during CRYSTAL-FACE. Journal of Geophysical Research - Atmospheres 108 (D20).

VanReken, T. M., N. L. Ng, R. C. Flagan and J. H. Seinfeld (2005). Cloud condensation nucleus activation properties of biogenic secondary organic aerosol. Journal Of Geophysical Research-Atmospheres 110(D7).

Wolff, G. T., Ruthosky, M. S., Stroup, D. P. and Korsog, P. E. (1991). A characterization of the principal PM-10 Species in Claremont (summer) and Long Beach (Fall) during SCAQS. Atmospheric Environment 25A: 2173-2186.

Table 1: Aqueous diffusivity of organic compounds found in atmospheric aerosols.

Compound	Molar mass ($g\ mol^{-1}$)	Formula	D_{Aw} (298 K) ($m^2\ s^{-1}$)	D_{Aw} (273 K) ($m^2\ s^{-1}$)
Sodium Chloride*	58.5	NaCl	1.26×10^{-9}	N/A
Methanol◊	24	CH_4O	1.94×10^{-9}	1.02×10^{-9}
Caffeine◊	150	$C_8H_{10}N_4O_2$	6.43×10^{-10}	3.38×10^{-10}
Adipic acid◊	114	$C_6H_{10}O_4$	8.19×10^{-10}	4.31×10^{-10}
Glutaric Acid◊	100	$C_5H_8O_4$	8.98×10^{-10}	8.73×10^{-10}
Succinic acid◊	86	$C_4H_6O_4$	1.00×10^{-9}	5.27×10^{-10}
Suberic◊	142	$C_8H_{14}O_4$	7.04×10^{-10}	3.70×10^{-10}
Cholesterol◊	378	$C_{27}H_{46}O$	3.73×10^{-10}	1.96×10^{-10}
C_{50} (e.g, humic-like substances) ◊	704	$C_{50}H_{104}$	2.47×10^{-10}	1.30×10^{-10}

* obtained from Perry, (1997). ◊ obtained from Hines, (1985).

Table 2: Parameters varied in numerical simulations.

D_{Aw} (m^2 s^{-1})	*s (%)* (Cloud type)	Drop Diameter (m)	$\frac{D_c}{D_p}$
1×10^{-10}	0	0.1×10^{-6}	0.005
2.5×10^{-10}	0.01 (fog)	0.5×10^{-6}	0.01
5×10^{-10}	0.25 (stratiform)	1.0×10^{-6}	0.05
1×10^{-9}	0.5 (cumulus)	5.0×10^{-6}	0.1
	1 (cumulus)	10.0×10^{-6}	0.2

Figure 1: Illustration of the problem geometry and the solute concentration profile. R_s represents the location where the concentration gradient becomes effectively zero.

Figure 2: Transient radial profiles of C_A. Simulations are shown for D_p = 1μm, D_c = 0.5μm, $D_{Aw} = 1\times10^{-10}$ m^2 s^{-1}, and s = 1%.

Figure 3: Steady-state radial profiles of C_A. Simulations are shown for D_p = 1μm, D_c = 0.01μm, s = 1%, and for D_{Aw} between 1×10^{-9} and 1×10^{-10} m^2 s^{-1}.

Figure 4: Steady-state radial profiles of C_A. Simulations are shown for D_p = 1μm, D_c = 0.01μm, $D_{Aw} = 1\times10^{-9}$ m^2 s^{-1}, and for s between 0.1% and 1%.

Figure 5: Steady-state droplet surface C_A normalized with C^{eq}, as a function of core diameter and ambient supersatuation. Simulations are shown for (a) D_p = 1μm, D_{Aw} = 1×10^{-10} m^2 s^{-1}, and, (b) D_p = 5μm, $D_{Aw} = 1\times10^{-9}$ m^2 s^{-1}.

Figure 6: Parameterized versus Simulated C^*. Simulations are shown for $C^* / C^{eq} \le 0.95$.

Figure 7: Köhler curves modified to include the effect of solute dissolution kinetics. The CCN dry diameter is 100 nm and composed of a partially soluble substance with 1750 kg m^{-3} density, 0.132 kg mol^{-1} molar mass, van't Hoff factor of 2 and a solubility of 10^{-2} kg kg^{-1}. Ambient supersaturation is assumed to be 1.0%. Calculations are presented as (a) s_{eq} vs. wet diameter for a range of D_{Aw}, and, (b) amount of partially soluble core left, expressed in terms of its diameter and % mass dissolved.

Figure 8: Köhler curves with (solid lines) and without (shaded lines) the effect of solute dissolution kinetics. The CCN have 100 nm dry diameter and are a mixture of NH_4HSO_4 and a partially soluble substance with the same properties as in Figure 7. Ambient supersaturation is assumed to be 1.0%, and $D_{Aw} = 7.5\times10^{-11}$ m^2 s^{-1}.

Figure 9: Sensitivity of C^* to the minimum C^* allowed in Equation 20. The conditions are similar to Figure 7. The inset graph displays the corresponding Köhler curves.

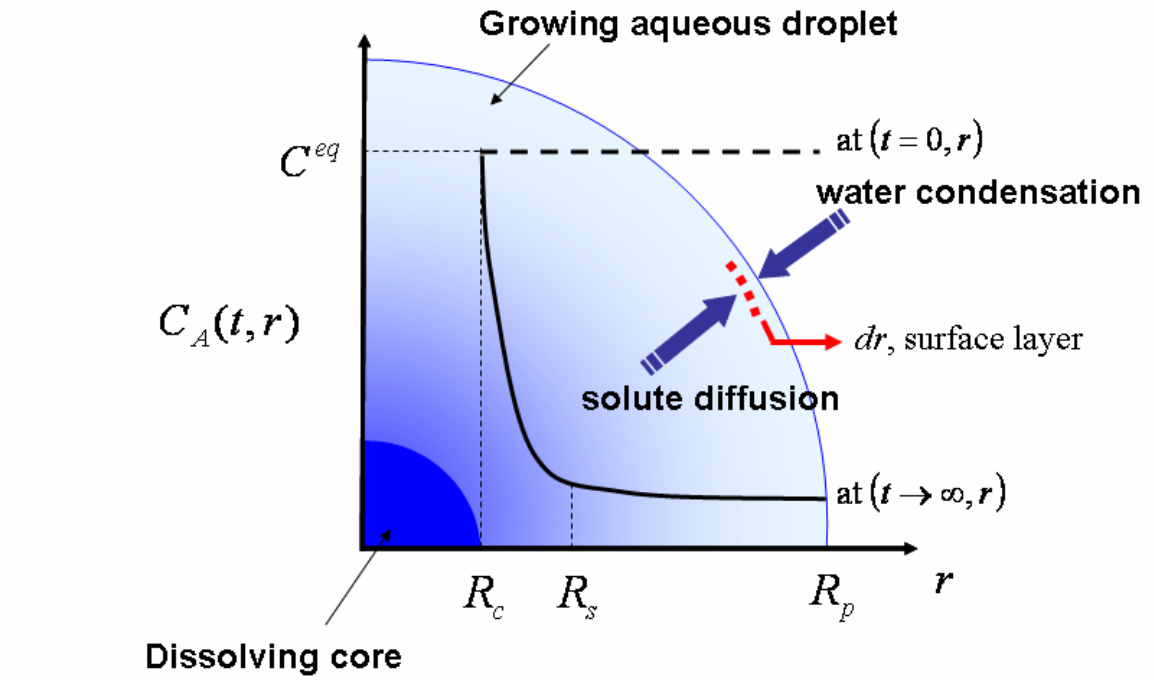
Growing aqueous droplet
C^{eq}
at $(t=0, r)$
water condensation
$C_A(t,r)$
dr, surface layer
solute diffusion
at $(t \to \infty, r)$
R_c
R_s
R_p
r
Dissolving core

Figure 1

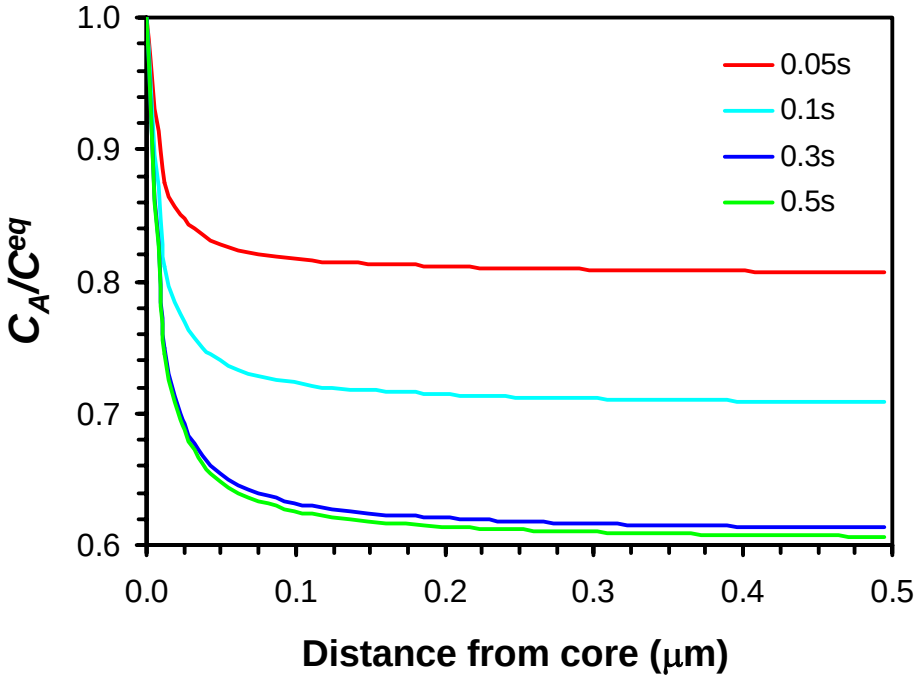
1.0
0.9
0.8
0.7
0.6
C_A/C^{eq}
0.0
0.1
0.2
0.3
0.4
0.5
Distance from core (μm)
0.05s
0.1s
0.3s
0.5s

Figure 2

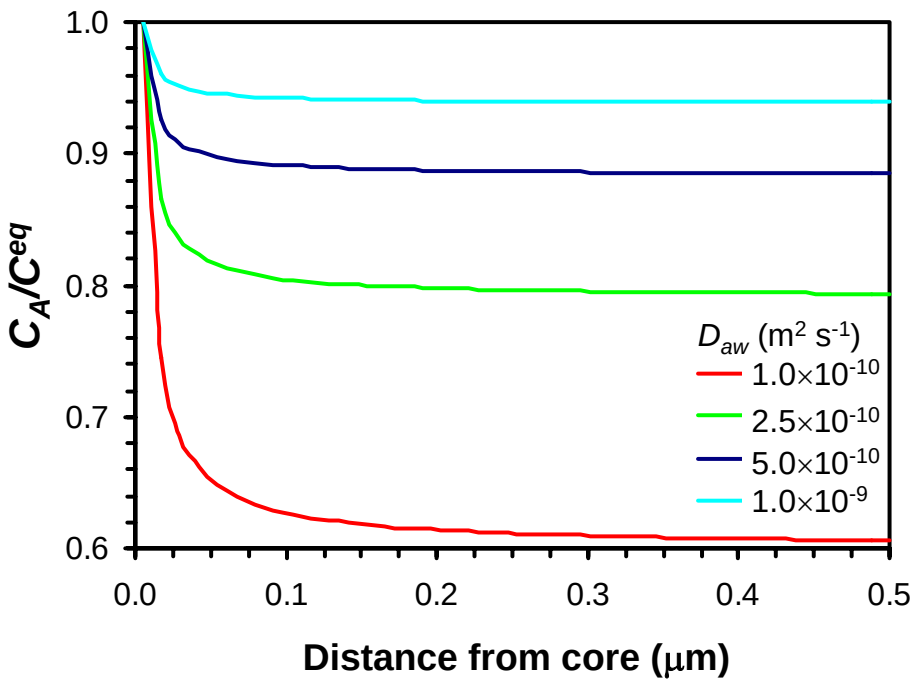
1.0
0.9
0.8
0.7
0.6
C_A/C^{eq}
0.0
0.1
0.2
0.3
0.4
0.5
Distance from core (μm)
D_{aw} (m^2 s^{-1})
1.0×10^{-10}
2.5×10^{-10}
5.0×10^{-10}
1.0×10^{-9}

Figure 3

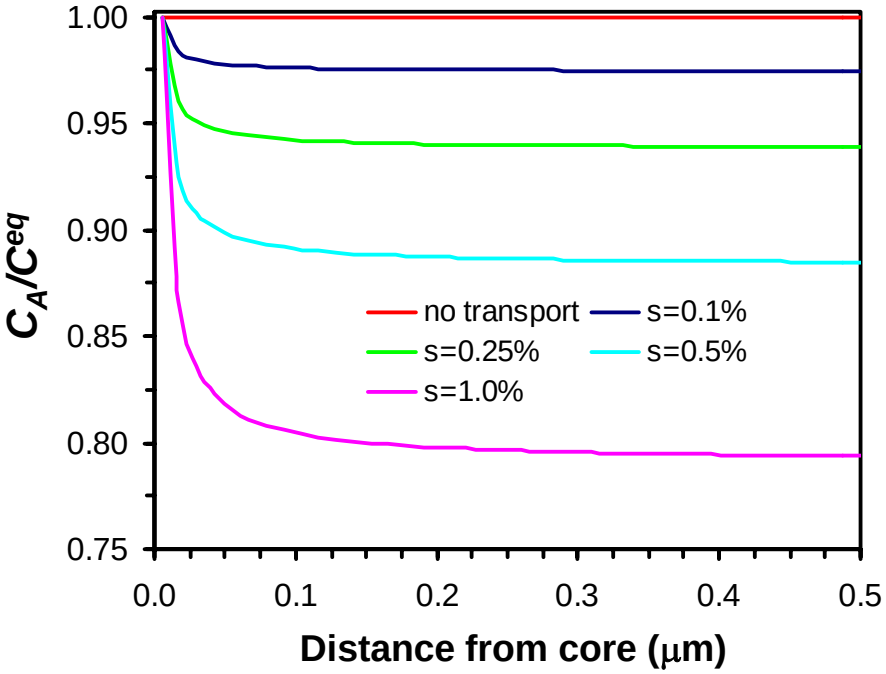
1.00
0.95
0.90
0.85
0.80
0.75
C_A/C^{eq}
no transport
s=0.1%
s=0.25%
s=0.5%
s=1.0%
0.0
0.1
0.2
0.3
0.4
0.5
Distance from core (μm)

Figure 4

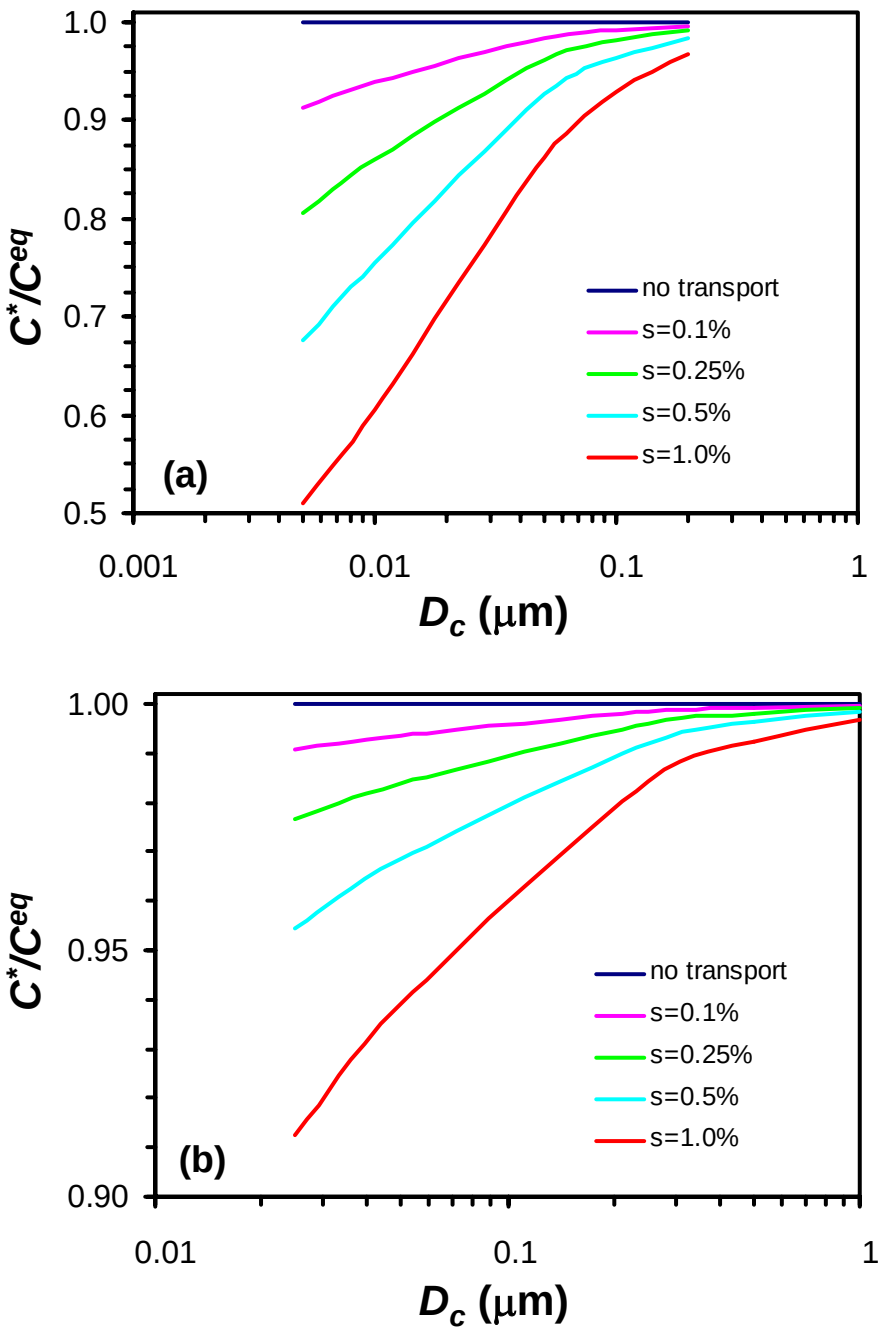
1.0
0.9
0.8
0.7
0.6
0.5
C*/Ceq
(a)
no transport
s=0.1%
s=0.25%
s=0.5%
s=1.0%
0.001
0.01
0.1
1
Dc (μm)
1.00
0.95
0.90
C*/Ceq
(b)
no transport
s=0.1%
s=0.25%
s=0.5%
s=1.0%
0.01
0.1
1
Dc (μm)

Figure 5

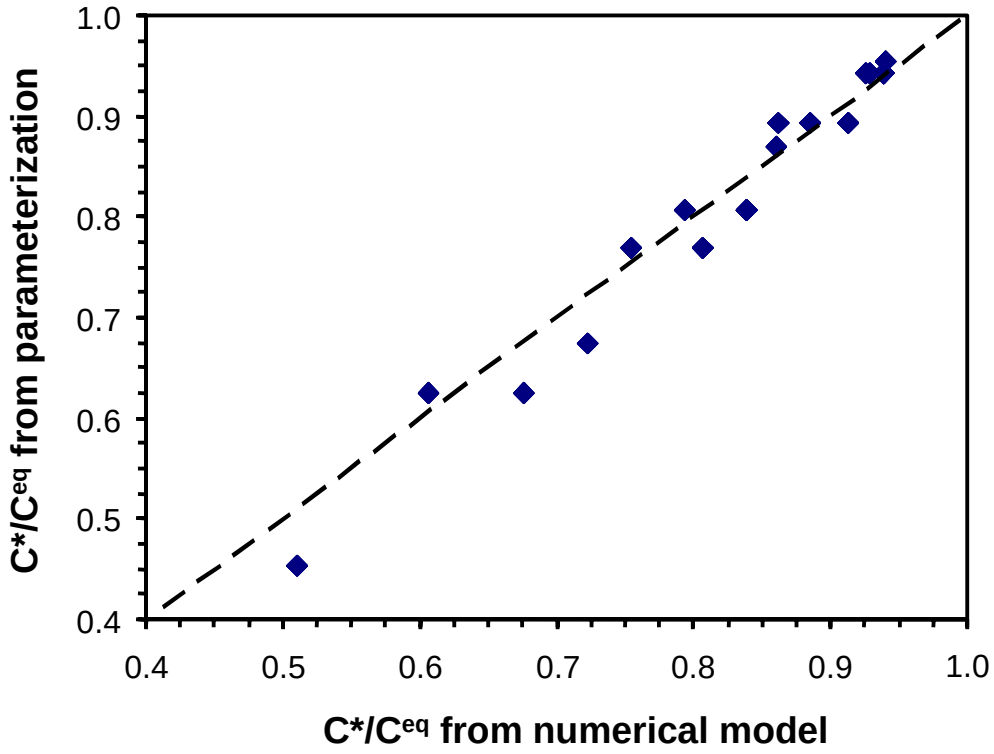
1.0
0.9
0.8
0.7
0.6
0.5
0.4
C*/Ceq from parameterization
0.4
0.5
0.6
0.7
0.8
0.9
1.0
C*/Ceq from numerical model

Figure 6

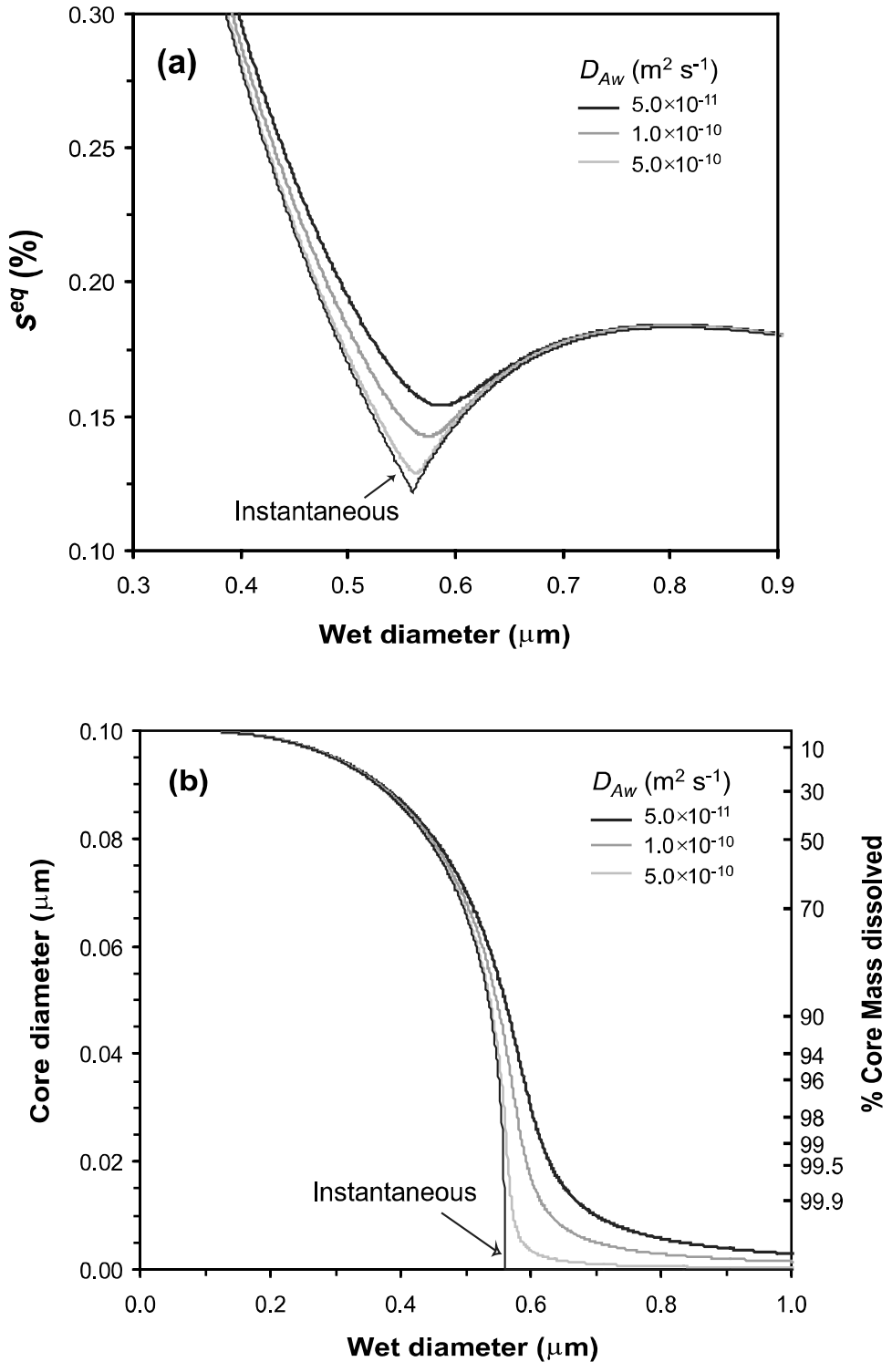
(a)
D_{Aw} (m^2 s^{-1})
5.0×10^{-11}
1.0×10^{-10}
5.0×10^{-10}
Instantaneous
s^{eq} (%)
Wet diameter (μm)
(b)
D_{Aw} (m^2 s^{-1})
5.0×10^{-11}
1.0×10^{-10}
5.0×10^{-10}
Instantaneous
Core diameter (μm)
% Core Mass dissolved
Wet diameter (μm)

Figure 7

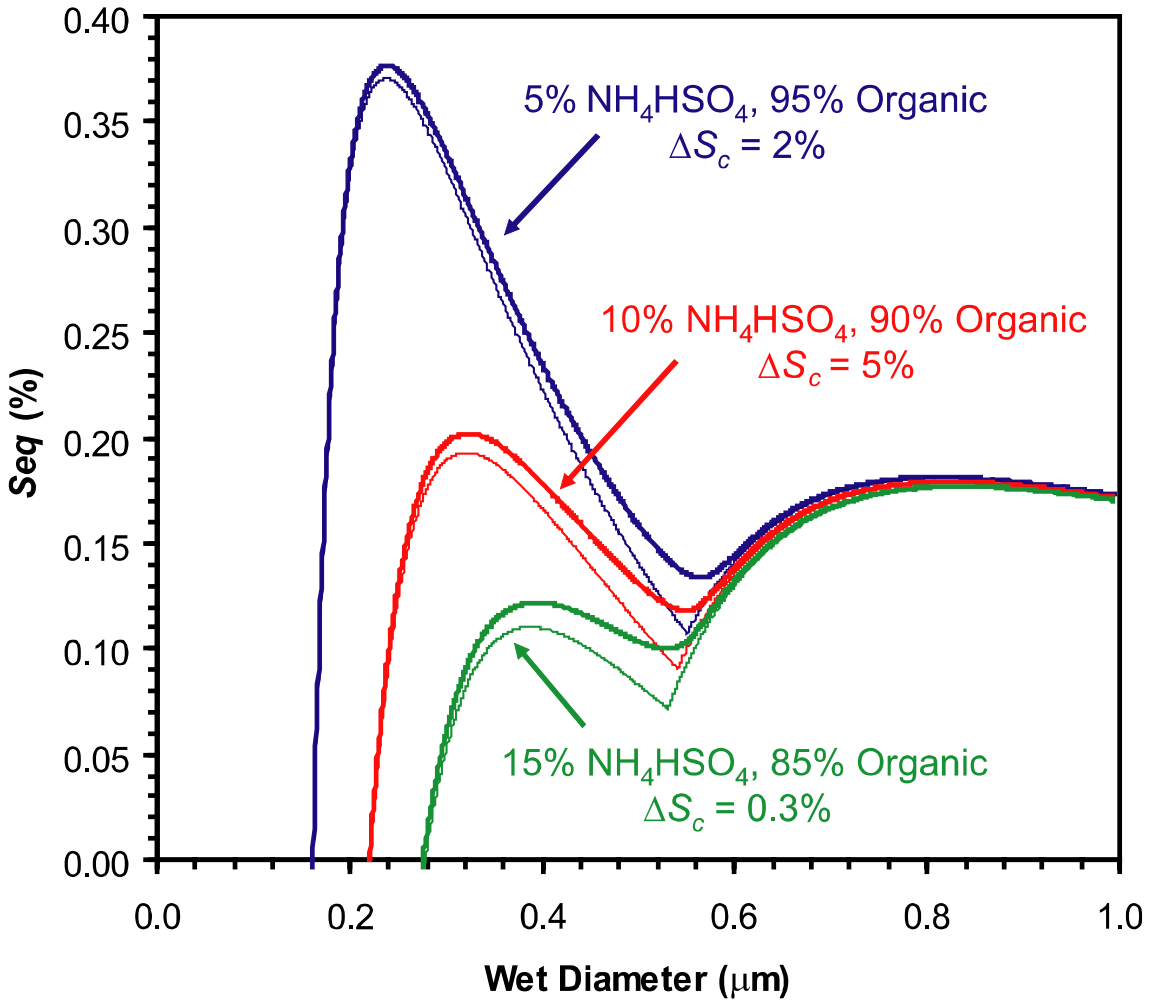
0.40
0.35
0.30
0.25
0.20
0.15
0.10
0.05
0.00
Seq (%)
0.0
0.2
0.4
0.6
0.8
1.0
Wet Diameter (μm)
5% NH4HSO4, 95% Organic
ΔSc = 2%
10% NH4HSO4, 90% Organic
ΔSc = 5%
15% NH4HSO4, 85% Organic
ΔSc = 0.3%

Figure 8

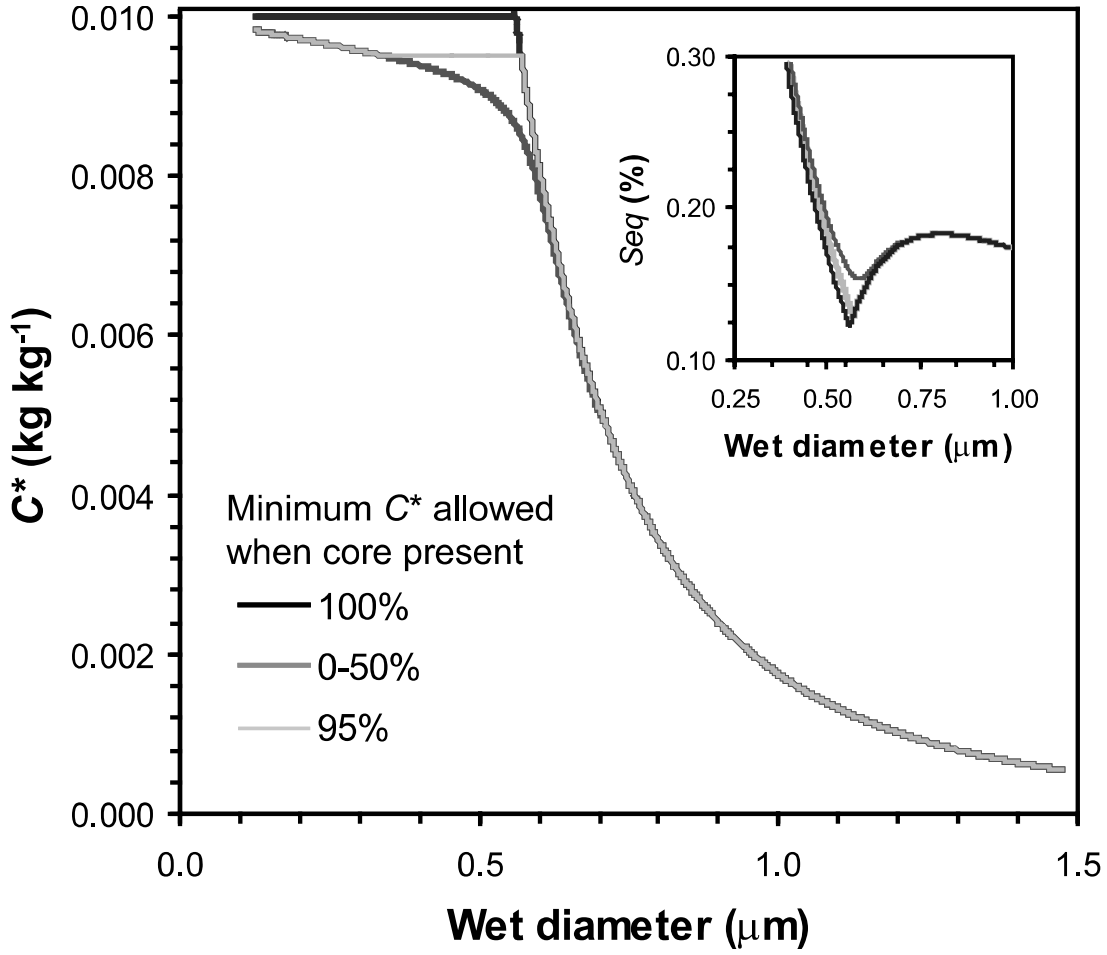
0.010
0.008
0.006
0.004
0.002
0.000
C* (kg kg-1)
0.0
0.5
1.0
1.5
Wet diameter (μm)
Minimum C* allowed
when core present
100%
0-50%
95%
0.30
0.20
0.10
Seq (%)
0.25
0.50
0.75
1.00
Wet diameter (μm)

Figure 9